Carbon nanofibers functionalized with active screen plasmadeposited metal nanoparticles for electrical energy storage devices

Corujeira Gallo, Santiago; Li, Xiaoying; Futterer, Klaus; Charitidis, Constantinos ; Dong, Hanshan

DOI:
10.1021/acsami.7b05567

Document Version
Peer reviewed version

Citation for published version (Harvard):
Corujeira Gallo, S, Li, X, Futterer, K, Charitidis, C & Dong, H 2017, 'Carbon nanofibers functionalized with active screen plasmadeposited metal nanoparticles for electrical energy storage devices', *ACS Applied Materials & Interfaces*, vol. 9, no. 27, pp. 23195-23201. https://doi.org/10.1021/acsami.7b05567

Carbon nanofibers functionalized with active screen plasma-deposited metal nanoparticles for electrical energy storage devices

Journal:	*ACS Applied Materials & Interfaces*
Manuscript ID	am-2017-05567x.R1
Manuscript Type:	Article
Date Submitted by the Author:	n/a
Complete List of Authors:	Corujeira-Gallo, Santiago; University of Birmingham, School of Metallurgy and Materials Li, Xiaoying; University of Birmingham, Metallurgy and Materials Fütterer, Klaus; University of Birmingham, School of Biosciences Charitidis, Constantinos; National Technical University of Athens, School of Chemical Engineering Dong, Hanshan; University of Birmingham, School of Metallurgy and Materials

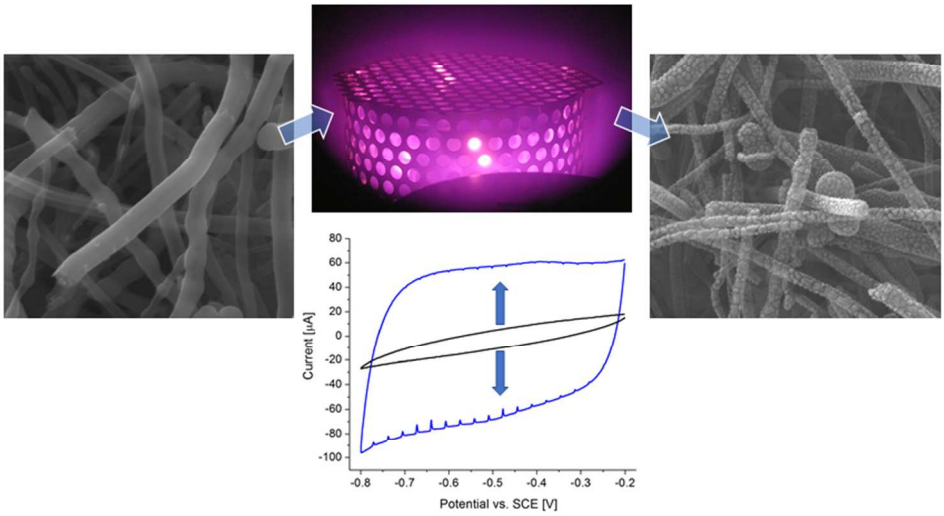

TOC. Graphical abstract.

237x133mm (96 x 96 DPI)

Carbon nanofibers functionalized with active screen plasma-deposited metal nanoparticles for electrical energy storage devices

Santiago Corujeira Gallo [a*], *Xiaoying Li* [a], *Klauss Futterer* [b], *Constantinos A. Charitidis* [c] *and Hanshan Dong* [a]

[a] School of Metallurgy and Materials, University of Birmingham

Edgbaston, Birmingham B15 2TT, United Kingdom.

[b] School of Biosciences, University of Birmingham

Edgbaston, Birmingham B15 2TT, United Kingdom.

[c] School of Chemical Engineering, National Technical University of Athens

Iroon Polytechneiou 9, Zografou 157 80, Greece.

[*]Corresponding author: Santiago Corujeira Gallo

Phone: +44 (0)121 414 5163

E-mail: corujeis@bham.ac.uk

ABSTRACT

Supercapacitors are energy storage devices with higher energy densities than conventional capacitors, but lower than batteries or fuel cells. There is a strong interest in increasing the volumetric and gravimetric capacitance of these devices to meet the growing demands of the electrical and electronic sectors. The capacitance depends largely on the electrode material, and carbon nanofibers (CNFs) have attracted much attention because of their relatively low cost, large surface area, good electrical conductivity as well as chemical and thermal stability. The deposition of metal nanoparticles on CNFs is a promising way to increase their surface properties and, ultimately, the capacitance of the devices. In this study, nickel and silver nanoparticles were deposited on CNFs using the active screen plasma technology. The CNFs were characterized and their electrochemical performance was assessed in a three electrode-cell. The results show significant improvements over the untreated CNFs, particularly after functionalization with silver nanoparticles.

KEYWORDS: carbon nanofibers; plasma; surface functionalization; electrochemistry; supercapacitors.

1. INTRODUCTION

In recent years, carbon nanofibers (CNFs) have attracted the attention of researchers for countless applications.[1] One example is the fabrication of electrodes for supercapacitors (SC), which are electrical devices used for storing energy.[2] The devices consist of two electrodes separated by an electrolyte,[3] and the principle of energy storage can be Faradic or non-Faradic, depending on their interaction.[4] Electrical double layer capacitors (EDLC) are based on non-Faradic mechanisms, in which the electric charge is stored in the double layer formed at the interface between the inert electrode material and the electrolyte, without involving redox reactions.[2] On the other hand, the

pseudo-capacitors (PsC) rely on reversible redox reactions (Faradic) which take place on the surface of the active electrode material in contact with the electrolyte.[5]

Supercapacitors can typically charge/discharge at higher rates than batteries and they have longer operating life, but their capacitance is limited.[1, 6] This limitation may be overcome by facilitating the charge exchange between the electrode material and the electrolyte, and the strategies to achieve this include: increasing the specific surface area,[2] optimizing the pore size,[6] increasing the electrical conductivity,[1] reactivity [7] or wettability [8] of the electrode material. The ideal electrode material for supercapacitors should combine the following chemical and physical properties:[2]

- high electrical conductivity
- high specific surface area
- good corrosion resistance
- high temperature stability
- controlled pore structure
- ease of processability and compatibility in composite materials
- low cost

Carbon materials meet most of these requirements,[2] and recent efforts have aimed to optimize the pore structure for a given electrolyte,[6] or to increase the surface reactivity with the addition of transition-metal oxides,[7] or both.[3] With this regard, carbon nanofibers (CNFs) and carbon nanotubes (CNTs) offer great versatility in terms of pore architecture [9] and they can act as scaffolds for more conductive or electroactive materials.[10] Ruthenium oxide has been extensively studied to increase the surface reactivity of CNFs and CNTs, but its practical use is hindered by high cost and environmental toxicity.[5] On the other hand, manganese oxides offer lower cost and environmental compatibility,[11] but lower electrical conductivity.[12] Nickel [13] and its oxides [14] have been proposed as electroactive materials, to superimpose pseudo-capacitance and double layer energy storage mechanisms in carbon based supercapacitors. The charge storage mechanism is based on surface adsorption of electrolyte cations C+ (K+, Na+…) as well as proton incorporation.[6] Additionally, the incorporation of silver

nanoparticles into PAN fibers was reported to increase their electrical conductivity and, ultimately, the capacitance of the device.[15] In this case, the charge is stored electrostatically using reversible adsorption of ions of the electrolyte onto the electrochemically stable and highly conductive material, with large specific surface area.[6] Regardless of the manufacturing process, the architecture consisting of a conductive or electroactive material deposited on the carbon nano-fibers was found to facilitate the diffusion of electrolyte ions, maximize the surface area for the electrochemical reaction and improve the charge percolation efficiency.[11]

Several multi-step processes use some kind of plasma technology to grow or etch nanostructures on carbon scaffolds,[16-17] or to modify the surface chemistry by reaction with gas species.[18-19] In this study, a simpler one-step surface engineering process, based on the advanced composite active screen technology, was used for the first time to functionalize carbon nanofibers. The surface morphology achieved with this technique, which consists of nanoparticles rather than smooth and continuous films, [20] increases the surface area significantly. In addition, the technology offers flexibility in terms of the metals and gas species which can be introduced. In this case, the plasma treatment conditions were optimized for nickel and silver nanoparticles, to assess the Faradic and non-Faradic charge storage mechanisms, respectively. The CNFs were characterized by scanning electron microscopy (SEM), transmission electron microscopy (TEM), energy dispersive X-ray spectroscopy (EDX) and X-ray diffraction (XRD) to assess their surface morphology, chemical composition and phase composition, respectively. In addition, cyclic voltammetry (CV) tests, cyclic charge-discharge (CCD) tests and electrochemical impedance spectroscopy (EIS) were conducted to assess the effectiveness of the plasma treatment. The results indicate that the capacitance of the cell increased considerably with the active screen plasma treatment, particularly for the CNFs functionalized with silver nanoparticles. The possible reasons for this improvement are discussed and the opportunities for further development of this novel technique are outlined.

2. EXPERIMENTAL PROCEDURES

The CNFs were acquired from Sigma-Aldrich (product No. 719811) and sonicated in isopropanol for 60 minutes to disperse them. The slurry was pipetted into clean borosilicate glass Petri dishes and the isopropanol was left to dry overnight. The Petri dishes with the dry residue of CNFs were introduced in the vacuum chamber of a Klockner Ionon plasma furnace fitted with a composite active screen (AS), in which nickel and silver plates were attached to the conventional AS set-up, respectively (Figure 1). The distance between the CNFs and the target plate of the active screen set-up was 15 mm. The chamber was evacuated to a base pressure below 1 Pa and the plasma treatments were conducted in a gas mixture consisting of 25% N_2 and 75% H_2 at a pressure of 75 Pa. The processing time was selected empirically, and varied between 15 minutes and 120 minutes to produce nanoparticles of different morphology, depending on the sputtering yield, nucleation and growth rate of each material (Table 1). The temperature was monitored with a K-type thermocouple inserted into a dummy block, and was limited to 400°C (±5°C) in all cases, to avoid damaging the Petri dishes (softening).

Table 1. Processing times selected for nickel and silver active screen arrangements.

Active screen material	Processing time 1	Processing time 2	Processing time 3
Nickel – AS(Ni)	15 minutes	30 minutes	60 minutes
Silver – AS(Ag)	30 minutes	60 minutes	120 minutes

The CNFs were fixed onto aluminum stubs using double sided adhesive carbon discs. The observations were conducted in a Jeol 7000 FEG-SEM, fitted with an Oxford Instruments Energy Dispersive X-ray (EDX) detector for chemical analysis. Some CNFs were transferred to copper grids and observed under a Jeol 2100 LaB6-TEM.

X-ray diffraction experiments were conducted in a Rigaku AFC11K SATURN 944 diffractometer with a micro-focus rotating copper anode operated at 40 kV and 30 mA (λ = 0.15418 nm). The detector was 93.7 mm x 93.7 mm in size (1042 x 1042 pixels), and the samples were positioned at a distance of 45 mm (resolution 0.09°). The CNFs were introduced in borosilicate glass capillaries with

a wall thickness of 0.01 mm. The system was calibrated using lanthanum hexaboride (LaB_6) powder and the background was corrected using an empty glass capillary. The exposure time was 10 s in all cases.

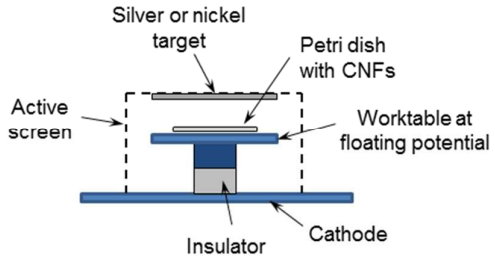

Figure 1. Experimental set-up for active screen plasma treatment.

The electrochemical assessment was conducted in a three electrode cell,[21] consisting of a platinum counter electrode, a saturated calomel reference electrode (SCE) and the CNF working electrode (Figure 2a). The loading of CNF on each electrode was 300 µg, measured with a OHAUS Galaxy 160D balance, and they were evenly distributed over an area of 28.3 mm^2 at the tip of the electrode (diameter = 6 mm). The potentiostat was a Gamry Instruments Interface 1000. The solution was made by dissolving sodium sulfate (Na_2SO_4), reagent grade, in deionized water to a 1M concentration, and the cell was kept at a constant temperature of 30°C ± 0.1°C using a Clifton thermostatic bath. Oxygen free argon was bubbled in the solution for 1 hour before the immersion of the sample and throughout the experiments. The samples were left to stabilize in the bath for 10 minutes before the measurements.

For the cyclic voltammetry (CV) tests, the working electrode was biased between -0.2 V and -0.8 V (± 0.01 V), versus the SCE reference electrode, at different rates: 25, 50, 100 and 200 mV/s. The cyclic charge/discharge (CCD) curves between -0.2 V and -0.8 V were collected at a constant current of 10 mA for 10 cycles. The electrochemical impedance spectra (EIS) were collected with a voltage

oscillation amplitude of 10 mV at frequencies between 0.01 Hz and 100 kHz. Figure 2b shows the equivalent circuit analog used to fit the experimental data,[22] in which the circuit elements are typically attributed to the resistance of the electrolyte (R_e), the charge transfer resistance (R_{ct}) and double layer capacitance (C_{dl}), the pseudo-capacitance (C_{ps}) and its associated resistance (R_{ps}). In this model, the capacitors C_{dl} and C_{ps} were modeled by constant phase elements, with exponents m and n, respectively, reflecting the departure of these circuit elements from ideal capacitors according to the following formula:

$$\frac{1}{Z_{CPE}} = Q.(i\omega)^{\alpha}$$

where Z_{CPE} is the impedance of the constant phase element, Q is the pre-factor, i is the imaginary unit, ω is the frequency and α is the exponent (n and m, for the two constant phase elements in Figure 2b).

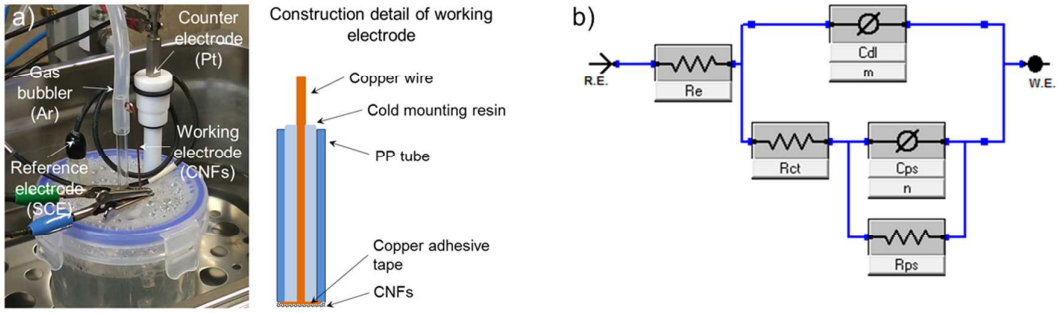

Figure 2. a) Experimental set-up used for the electrochemical tests and b) Electric circuit analog. R_e: electrolyte resistance; R_{ct}: charge transfer resistance; C_{dl}: double layer capacitance and exponent of the constant phase element (m); R_{ps}: resistance of pseudo-capacitance; C_{ps}: pseudo-capacitance and exponent of the constant phase element (n).

All the electrochemical tests were replicated a minimum of 5 times and the results presented in this article correspond to the most representative curves or the average values. It should be emphasized that these experiments, conducted in a three-electrode cell, do not simulate a supercapacitor device.

As a consequence, the results are a qualitative comparison between CNFs with different surface treatments, but the data should not be extrapolated to real supercapacitor devices, which are likely to have a different geometrical set-up and exhibit lower contact resistance between the active material (CNFs) and the current collector.

3. RESULTS AND DISCUSSION

Characterization of functionalized CNFs

Figure 3 illustrates the differences observed on the CNFs before and after the active screen surface functionalization. The untreated material consisted of fibers with a mean diameter between 100 nm and 200 nm, which exhibited a smooth surface morphology. The TEM observations revealed the hollow nature of these fibers, which resembles CNTs. Moreover, a 'stacked-cup' structure was observed along the fiber axis. The active screen surface functionalization did not affect the size or the structure of the CNFs, but the surface morphology was significantly altered. The SEM micrograph in Figure 3b shows a high density of particles on the surface of the CNFs. The deposited particles are also visible in the TEM micrograph in Figure 3d, having a diameter which typically varies between 10 nm and 50 nm. More importantly, the latter image shows that the deposition is not uniform and the particle density differs from fiber to fiber.

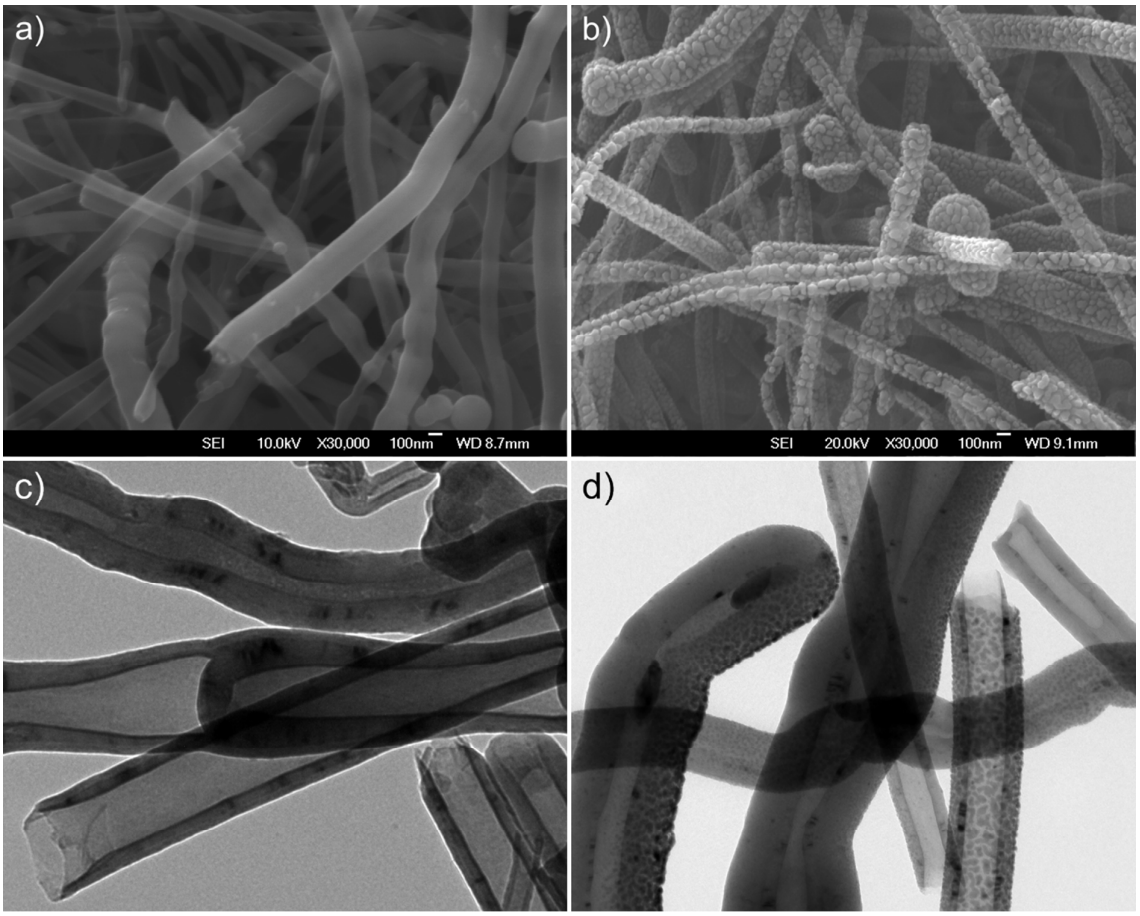

Figure 3. SEM and TEM images of: a) and c) untreated CNFs and b) and d) active screen plasma functionalized CNFs: AS(Ni)2.

Figure 4 shows the EDX spectra, in which the presence of nickel and silver can be clearly identified on the CNFs after the active screen plasma treatments. The density and size of the deposited particles changed with the sputtered material and with the processing time. The AS(Ni) CNFs in Figure 5a exhibit the same smooth morphology of the untreated CNFs, and there were no signs of nickel on their surface. On the other hand, the CNFs treated for longer times exhibited small particles on their surface (Figure 5b and 5c), which were rich in nickel. The nanoparticles grew larger with increasing processing time and they became uneven in size and shape after 60 minutes of plasma treatment.

The morphology of the CNFs functionalized with silver was quite different, and the deposited nanoparticles were very small but uniform after 30 minutes of active screen plasma treatment (Figures

5d). With increasing processing time, the particles became coarser and coalesced, to cover the full surface of the CNFs. In spite of this, the surface morphology remained uniform, even after 2 hours of plasma treatment (Figures 5e and 5f).

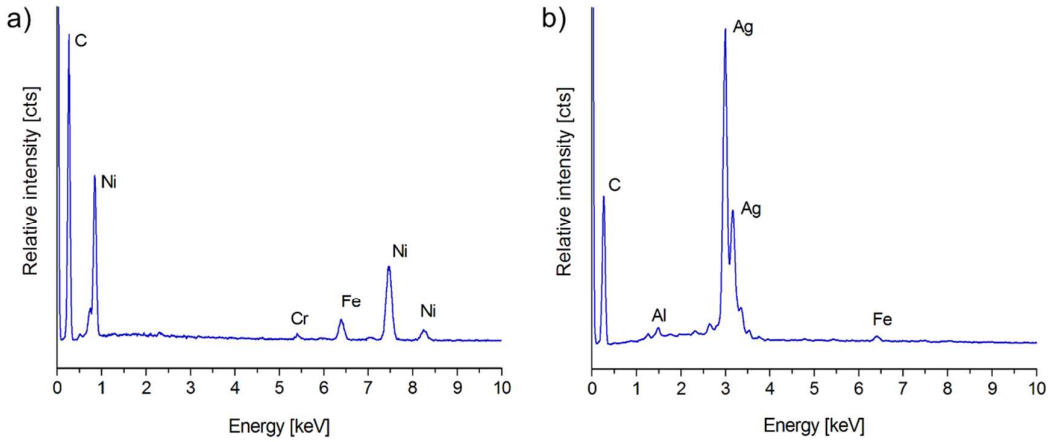

Figure 4. EDX results corresponding to: a) AS(Ni) and b) AS(Ag) functionalized CNFs

The X-ray diffraction traces also revealed differences between the AS(Ni) and the AS(Ag) CNFs (Figure 6). The CNFs functionalized with nickel exhibited a diffraction pattern comparable to the untreated material, with the typical turbostratic carbon ring and only one faint ring attributed to nickel (111). The ring is blurred, which reflects the low content and uneven layer of nickel on the CNFs. What is more, this peak appears shifted to lower angle compared to the reference pattern, possibly indicating the introduction of interstitial nitrogen in the nickel structure. The elucidation of this phenomenon requires further work.

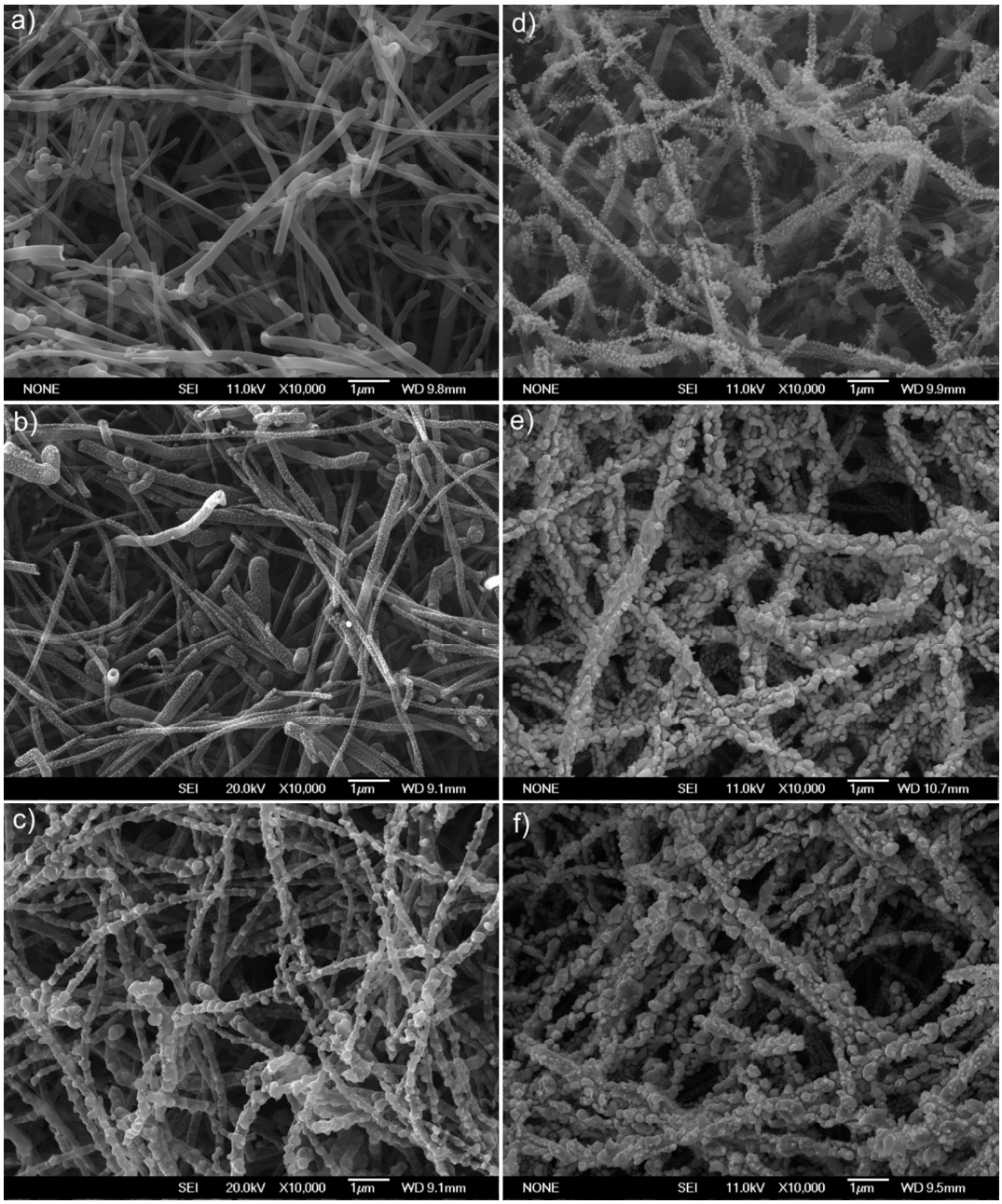

Figure 5. SEM micrographs of active screen plasma functionalized CNFs:

AS(Ni): a) 15 min., b) 30 min., and c) 60 min.;

AS(Ag): d) 30 min., e) 60 min., and f) 120 min.

In contrast, the CNFs functionalized with silver produced two clear diffraction rings corresponding to the (111) and (200) planes. Moreover, the intensity of these diffraction rings increased with the treatment time, reflecting the increase in the silver content on the surface of the CNFs.

These results indicate that the AS(Ag) CNFs had a higher content of metal particles on their surface compared with their AS(Ni) counterparts. This could be attributed to the shorter processing time used for AS(Ni) and the lower sputtering yield of nickel, compared to silver.[23] Unfortunately, the surface morphology obtained after longer AS(Ni) treatments was excessively uneven, and this condition was rejected in favor of the ones which produced smaller and more uniform particles on the CNFs. On the other hand, the silver particles deposited on the CNFs became coarser with increasing treatment time, but their size remained uniform and, consequently, they were considered more suitable for the electrochemical assessment.

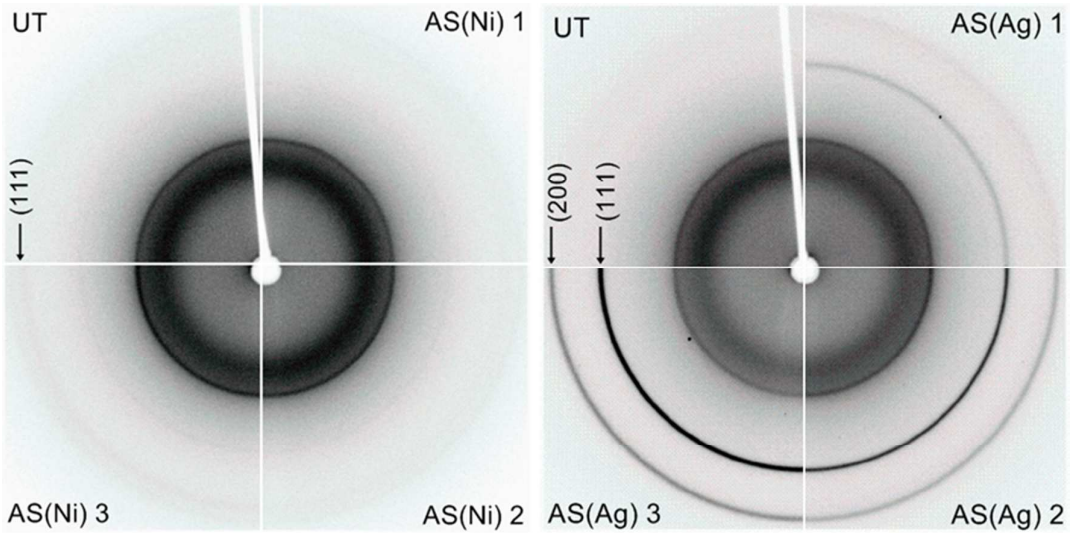

Figure 6. X-ray diffraction traces corresponding to: UT, AS(Ni) and AS(Ag) CNFs.

In both cases, AS(Ni) and AS(Ag), the sputtering of material from the target and its re-deposition on the CNFs is a line-of-sight process. Therefore, the CNFs which are closer to the target are expected to develop larger particles or thicker deposition layers than the CNFs which are further away or partially

covered. Figure 5 shows nickel or silver nanoparticles beyond the first layer of CNFs, but a careful observation reveals that their size is smaller in partially covered areas, compared to the most exposed areas; this difference is a result of the shadowing effect mentioned before. The shadowing effect would be more significant for AS(Ni) because of the lower sputtering yield and throwing power of nickel, compared to silver.

The faint rings observed in the X-ray diffraction traces of AS(Ni) CNFs is another indication of the uneven surface treatment, which contrasts with the continuous layer of nickel particles observed under the SEM on these same CNFs. The conflicting results obtained by SEM (surface sensitive) and XRD (bulk sensitive) indicate that further improvements in the active screen plasma processing conditions should aim to produce a uniform surface functionalization of the CNFs, particularly when using materials with low sputtering yield.

Electrochemical testing

Figure 7 shows the cyclic voltammetry results obtained using CNFs with different surface conditions. The AS(Ni) 1 sample showed the same response as the untreated CNFs (UT) with a rather small loop area but with little distortion from the rectangular shape, even at high scan rates. The curves of CNFs treated for longer time, AS(Ni) 2 and AS(Ni) 3, exhibited marginally larger loop areas, which are indicative of higher capacity, but the curves deviated from the rectangular shape and appeared distorted at high scan rates, which is attributed to the low ion transport efficiency.[12] On the other hand, all the CV curves obtained with AS(Ag) CNFs exhibited a considerably larger loop area, which increased with the processing time: AS(Ag) 1 < AS(Ag) 2 < AS(Ag) 3. In addition, the curves retained their rectangular shape, even at high scanning rates, which is a result of the high surface conductivity and ion transport efficiency obtained with the Ag nanoparticles on the CNFs.

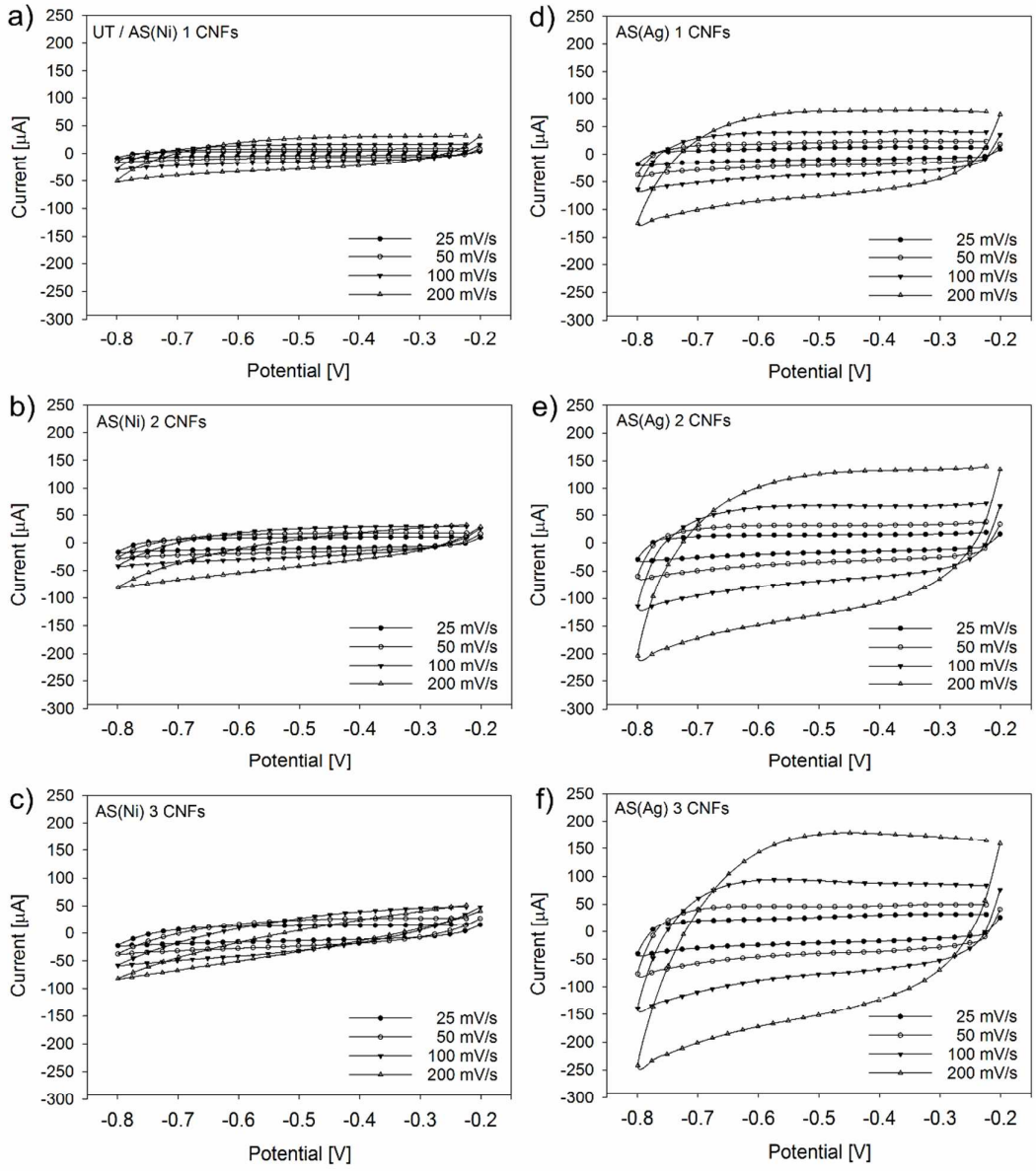

Figure 7. Cyclic voltammetry tests conducted on functionalized CNTs:

a) UT / AS(Ni) 1, b) AS(Ni) 2, c) AS(Ni) 3, d) AS(Ag) 1, e) AS(Ag) 2 and f) AS(Ag) 3.

The differences in surface condition were also reflected on the cyclic charge-discharge (CCD) results. Figure 8a shows the CCD curves obtained with the CNF electrodes in their maximum functionalization conditions, AS(Ni) 3 and AS(Ag) 3, compared to the untreated material (UT). The charge and discharge times were clearly longer for AS(Ni) 3 and AS(Ag) 3 CNFs, indicating that

these electrodes could accommodate higher levels of electric charge. The curves retained their triangular shape and appeared quite symmetrical, although there were signs of distortion at the end of the charging cycle, which indicate an increase in the diffusion resistance. The IR drop visible at the vertex of each charge-discharge cycle was moderate in all cases, but smaller for the functionalized CNFs compared to the UT electrodes. This was particularly true for the AS(Ag) electrodes, and indicates a lower equivalent series resistance (ESR).

A summary of the results from the CCD tests is presented in Figure 8b, which illustrates the difference between the AS functionalized CNFs and the untreated material. This figure also reveals a significant scattering in the data, which was attributed to the uneven functionalization with nickel and silver nanoparticles, as described above. However, the differences observed for most of the functionalized conditions are unquestionably higher than the UT material.

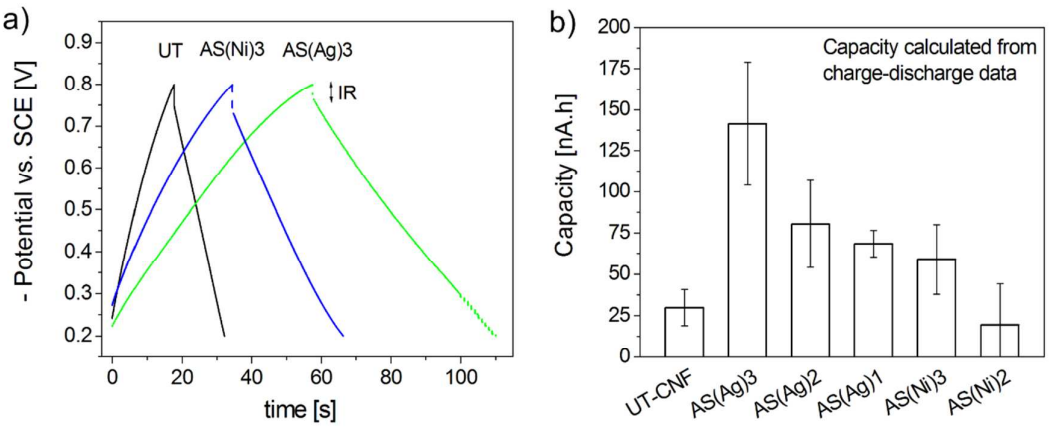

Figure 8. a) Cyclic charge-discharge curves (10 mA); and b) calculated capacity for CNFs with different surface conditions.

The electrochemical impedance spectra (EIS) exhibited a similar trend and some characteristic curves are shown in Figure 9. The high values of Z are attributed to the experimental set-up, particularly the double-sided copper tape used as collector. Nevertheless, the shape of the curves is consistent with the

proposed electric circuit analog model, and the fitting parameters are summarized in Table 2. Samples AS(Ni) 1 and AS(Ni) 2 produced inconsistent results, which was attributed to the poor and uneven coverage of the CNFs with nickel nanoparticles. Moreover, the EIS and the fitting values corresponding to these two samples were comparable to the UT CNFs. Therefore, these results were excluded from Table 2. However, this is noteworthy given that the N_2 and H_2 plasma are known to introduce polar functional groups on carbon substrates, which increase their wettability in aqueous solutions.[24] Therefore, the lack of improvement observed on AS(Ni)1 and AS(Ni) 2 samples indicates that the N_2 and H_2 plasma by itself, i.e. without the deposition of metal nanoparticles, was insufficient to improve the electrochemical performance of the CNF electrodes.

Table 2. Summary of electric circuit analog parameters used to fit the EIS results

Circuit element	Untreated	AS(Ni) 3	AS(Ag) 1	AS(Ag) 2	AS(Ag) 3
R_{ct} [a]	1	0.71	0.88	0.84	0.37
C_{dl} [a]	1	0.7	4.65	2.22	7.70
n	0.91	0.79	0.86	0.86	0.93
R_{ps} [a]	1	0.14	>1E^3	>1E^3	>1E^3
C_{ps} [a]	1	0.38	0.62	0.27	0.59
m	0.6	0.59	0.48	0.44	0.38

[a] Values relative to the untreated carbon nanofibers.

On the other hand, the AS(Ni) 3 and all the AS(Ag) CNFs showed clear differences compared with the UT CNFs. The functionalization with nickel decreased R_{ps} significantly, which was attributed to Faradic mechanisms associated with the electroactive layer of nickel, although the values of both C_{dl} and C_{ps} dropped. In the low-frequency section, the curve also shows a lower slope which indicates a low ion transport efficiency. In contrast, the functionalization with silver reduced R_{ct} and increased C_{dl}, which is consistent with the non-Faradic mechanism of electric charge storage. In addition, R_{ps} increased relative to the UT CNF electrodes. In both cases, the values of exponents *n* and *m* were quite low, particularly for *m* (associated with C_{ps}), which indicates a deviation from the ideal

capacitor. The reasons for this deviation are not known, but it has been attributed to the physical and chemical heterogeneity of the electrode surface.

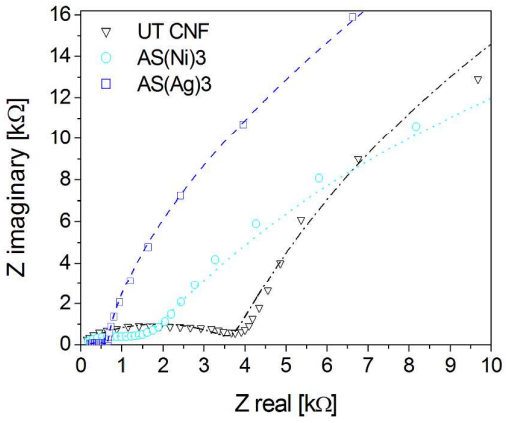

Figure 9. Electrochemical impedance spectra of UT, AS(Ni)3 and AS(Ag)3 CNF electrodes.

The results presented in this article show that the largest increase in capacity was achieved with the highly conductive silver nanoparticles, rather than the electroactive nickel nanoparticles. This seems to indicate that the increase in capacity was mainly achieved by the double layer, rather than the pseudo-capacitance. However, it was recently reported that vanadium and other transition metal nitrides can improve both Faradic and non-Faradic charge storage mechanisms, which make them promising electrode materials for supercapacitors.[25-26] This finding opens good prospects for the active screen plasma technology, considering that it has been extensively used to form nitrides and carbides for surface functionalization and hardening. However, the processing conditions will need to be optimized to obtain nanoparticles of the required size and shape and to functionalize the carbon nanofibers evenly. With this regard, the use of modified reactors which stir the CNFs during the process is promising, [27] but it poses technical challenges as well as health and safety concerns due to airborne CNFs.[28] Alternatively, the plasma treatment could be conducted on the finished electrodes made of thin CNF mats, rather than on loose CNFs. In this way, the nanoparticles would mainly form

on the surface exposed to the electrolyte, where they are most effective, but they may also reduce the surface area by clogging the porosity of the mat.

4. CONCLUSIONS

The surface functionalization of carbon nanofibers with the active screen plasma technology produced the following results:

- It was possible to form silver and nickel nanoparticles on the surface of carbon nanofibers, although the treatment was not entirely uniform.
- The nanoparticles varied in size and morphology depending on the processing conditions and the deposited material; this is associated with the sputtering yield and processing time.
- The electrochemical response of the functionalized carbon nanofibers shows an increase in capacity, although the results bare considerable error because of the lack of treatment uniformity.
- The increase in performance was particularly significant for the nanofibers functionalized with silver, based on a double layer storage, rather than a pseudo-capacitance mechanism;

The recent findings on transition metal nitrides for improved Faradic and non-Faradic charge storage mechanisms open very good opportunities for the active screen plasma technology.

ACKNOWLEDGMENTS

The research leading to these results has received funding from the European Union's Seventh Framework Program (FP7/2007-2013) under the agreement N° GA604248.

REFERENCES

1. Aricò, A. S.; Bruce, P.; Scrosati, B.; Tarascon, J. M.; Van Schalkwijk, W., Nanostructured Materials for Advanced Energy Conversion and Storage Devices. *Nat Mater* **2010,** *4*, 366-377.

2. Pandolfo, A. G.; Hollenkamp, A. F., Carbon Properties and Their Role in Supercapacitors. *J Power Sources* **2006,** *157* (1), 11-27.

3. Simon, P.; Gogotsi, Y., Materials for Electrochemical Capacitors. *Nat Mater* **2008,** *7* (11), 845-854.

4. González, A.; Goikolea, E.; Barrena, J. A.; Mysyk, R., Review on Supercapacitors: Technologies and Materials. *Renew Sust Energ Rev* **2016,** *58*, 1189-1206.

5. Liu, J.; Essner, J.; Li, J., Hybrid Supercapacitor Based on Coaxially Coated Manganese Oxide on Vertically Aligned Carbon Nanofiber Arrays. *Chem Mater* **2010,** *22* (17), 5022-5030.

6. Simon, P.; Gogotsi, Y., Charge Storage Mechanism in Nanoporous Carbons and Its Consequence for Electrical Double Layer Capacitors. *Philos T R Soc A* **2010,** *368* (1923), 3457-3467.

7. Zhu, Y.; Murali, S.; Stoller, M. D.; Ganesh, K. J.; Cai, W.; Ferreira, P. J.; Pirkle, A.; Wallace, R. M.; Cychosz, K. A.; Thommes, M.; Su, D.; Stach, E. A.; Ruoff, R. S., Carbon-Based Supercapacitors Produced by Activation of Graphene. *Science* **2011,** *332* (6037), 1537-1541.

8. Yoon, B. J.; Jeong, S. H.; Lee, K. H.; Seok Kim, H.; Gyung Park, C.; Hun Han, J., Electrical Properties of Electrical Double Layer Capacitors with Integrated Carbon Nanotube Electrodes. *Chem Phys Lett* **2004,** *388* (1-3), 170-174.

9. Wang, X.; Jiang, K.; Shen, G., Flexible Fiber Energy Storage and Integrated Devices: Recent Progress and Perspectives. *Mater Today* **2015,** *18* (5), 265-272.

10. Mao, X.; Rutledge, G. C.; Hatton, T. A., Nanocarbon-Based Electrochemical Systems for Sensing, Electrocatalysis, and Energy Storage. *Nano Today* **2014,** *9* (4), 405-432.

11. Ghodbane, O.; Louro, M.; Coustan, L.; Patru, A.; Favier, F., Microstructural and Morphological Effects on Charge Storage Properties in Mno2-Carbon Nanofibers Based Supercapacitors. *J Electrochem Soc* **2013,** *160* (11), A2315-A2321.

12. Yang, C.; Zhou, M.; Xu, Q., Three-Dimensional Ordered Macroporous Mno<Inf>2</Inf>/Carbon Nanocomposites as High-Performance Electrodes for Asymmetric Supercapacitors. *Phys Chem Chem Phys* **2013,** *15* (45), 19730-19740.

13. Li, J.; Liu, E. h.; Li, W.; Meng, X. y.; Tan, S. t., Nickel/Carbon Nanofibers Composite Electrodes as Supercapacitors Prepared by Electrospinning. *J Alloy Compd* **2009,** *478* (1-2), 371-374.

14. Tai, Y. L.; Teng, H., Modification of Porous Carbon with Nickel Oxide Impregnation to Enhance the Electrochemical Capacitance and Conductivity. *Carbon* **2004,** *42* (11), 2335-2338.

15. Park, S. J.; Im, S. H., Electrochemical Behaviors of Pan/Ag-Based Carbon Nanofibers by Electrospinning. *B Kor Chem Soc* **2008,** *29* (4), 777-781.

16. Haniff, M. A. S. M.; Hafiz, S. M.; Wahid, K. A.; Endut, Z.; Syono, M. I.; Huang, N. M.; Rahman, S. A.; Azid, I. A., Nitrogen-Doped Multiwalled Carbon Nanotubes Decorated with Copper(I) Oxide Nanoparticles with Enhanced Capacitive Properties. *J Mater Sci* **2017,** *52* (11), 6280-6290.

17. Tali, S. A. S.; Soleimani-Amiri, S.; Sanaee, Z.; Mohajerzadeh, S., Nitrogen-Doped Amorphous Carbon-Silicon Core-Shell Structures for High-Power Supercapacitor Electrodes. *Sci Rep-UK* **2017,** *7*, 1-13.

18. Liang, H.; Xia, C.; Jiang, Q.; Gandi, A. N.; Schwingenschlögl, U.; Alshareef, H. N., Low Temperature Synthesis of Ternary Metal Phosphides Using Plasma for Asymmetric Supercapacitors. *Nano Energy* **2017,** *35*, 331-340.

19. Lee, G.; Lee, C.; Yoon, C. M.; Kim, M.; Jang, J., High-Performance Three-Dimensional Mesoporous Graphene Electrode for Supercapacitors Using Lyophilization and Plasma Reduction. *ACS Appl Mater Interfaces* **2017,** *9* (6), 5222-5230.

20. Li, C. X.; Bell, T.; Dong, H., A Study of Active Screen Plasma Nitriding. *Surf Eng* **2002,** *18* (3), 174-181.

21. ASTM G5; Standard Reference Test Method for Making Potentiodynamic Anodic Polarization Measurements; **2014**; pp 1-9.

22. Fisher, R. A.; Watt, M. R.; Jud Ready, W., Functionalized Carbon Nanotube Supercapacitor Electrodes: A Review on Pseudocapacitive Materials. *ECS J Solid State Sc* **2013,** *2* (10), M3170-M3177.

23. Laegreid, N.; Wehner, G. K., Sputtering Yields of Metals for Ar+ and Ne+ Ions with Energies from 50 to 600 Ev. *J. Appl. Phys.* **1961,** *32* (3), 365-369.

24. Corujeira Gallo, S.; Charitidis, C.; Dong, H., Surface Functionalization of Carbon Fibers with Active Screen Plasma. *J Vac Sci Technol A* **2017,** *35* (2), 021404-021401-021410.

25. Yang, Y.; Shen, K.; Liu, Y.; Tan, Y.; Zhao, X.; Wu, J.; Niu, X.; Ran, F., Novel Hybrid Nanoparticles of Vanadium Nitride/Porous Carbon as an Anode Material for Symmetrical Supercapacitor. *Nano-Micro Letters* **2017,** *9* (1).

26. Balogun, M. S.; Qiu, W.; Wang, W.; Fang, P.; Lu, X.; Tong, Y., Recent Advances in Metal Nitrides as High-Performance Electrode Materials for Energy Storage Devices. *Journal of Materials Chemistry A* **2015,** *3* (4), 1364-1387.

27. Brüser, V.; Heintze, M.; Brandl, W.; Marginean, G.; Bubert, H., Surface Modification of Carbon Nanofibres in Low Temperature Plasmas. *Diam Relat Mater* **2004,** *13* (4-8), 1177-1181.

28. NIOSH; DHHS No 2012–147; General Safe Practices for Working with Engineered Nanomaterials in Research Laboratories; **2012**; pp 1-60.

TOC GRAPHICAL ABSTRACT

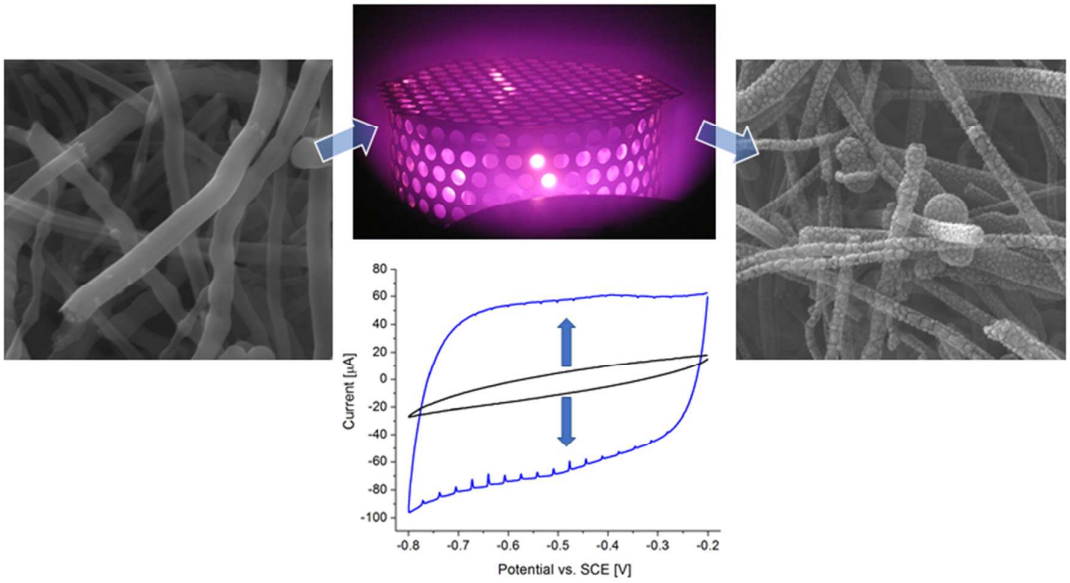

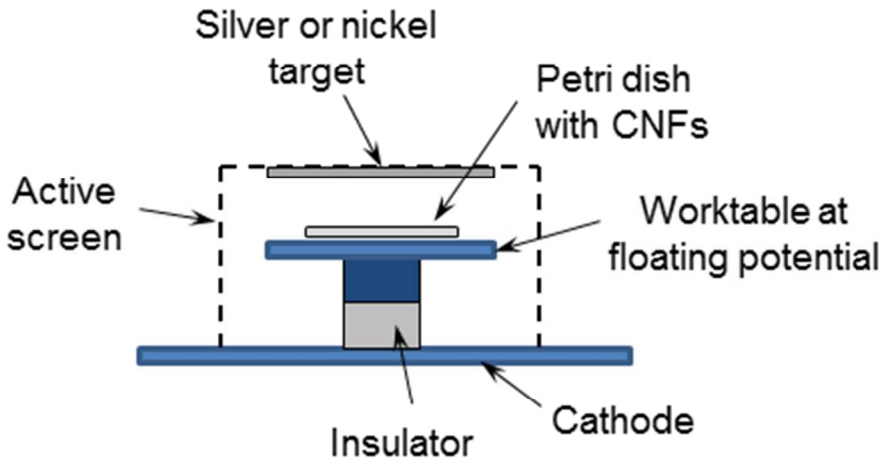

Figure 1. Experimental set-up for active screen plasma treatment.

127x73mm (96 x 96 DPI)

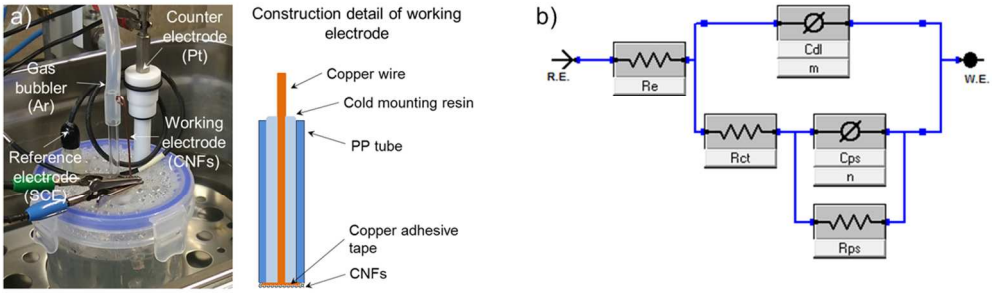

Figure 2. a) Experimental set-up used for the electrochemical tests and b) Electric circuit analog.

333x99mm (96 x 96 DPI)

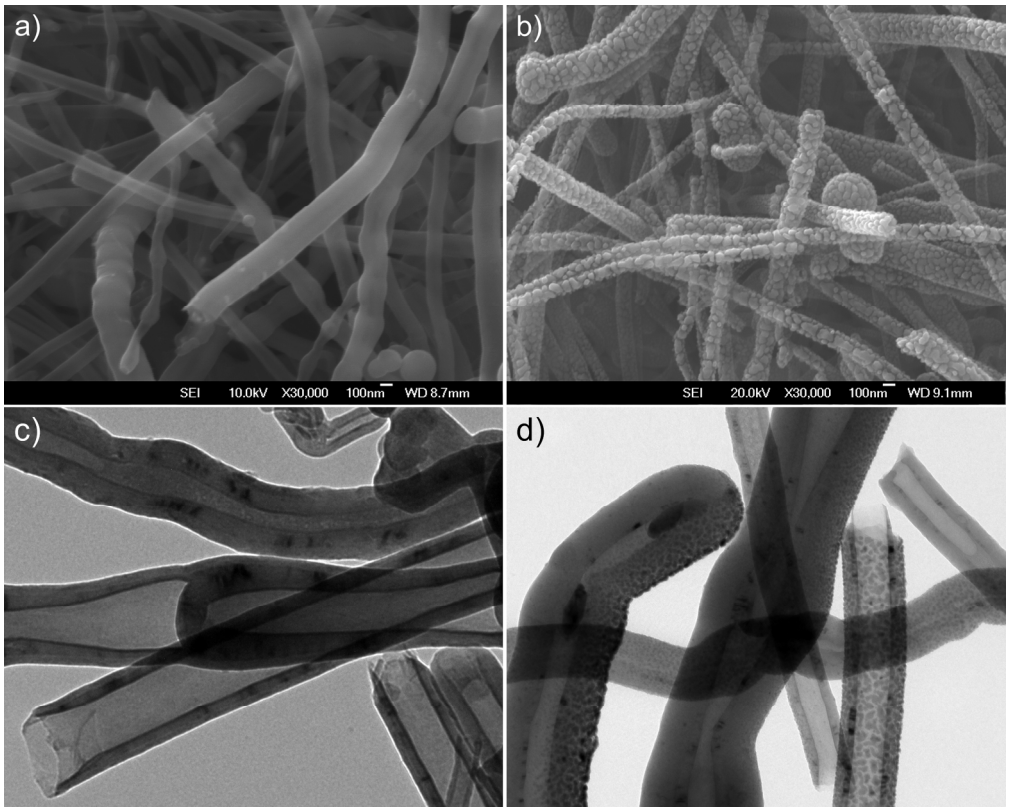

Figure 3. SEM and TEM images of: a) and c) untreated CNFs and b) and d) active screen plasma functionalized CNFs: AS(Ni)2.

577x462mm (96 x 96 DPI)

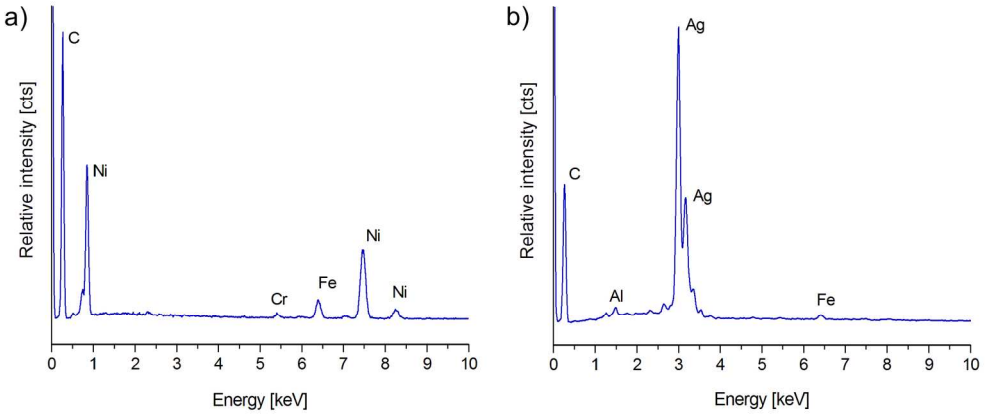

Figure 4. EDX results corresponding to: a) AS(Ni) and b) AS(Ag) functionalized CNFs.

609x258mm (96 x 96 DPI)

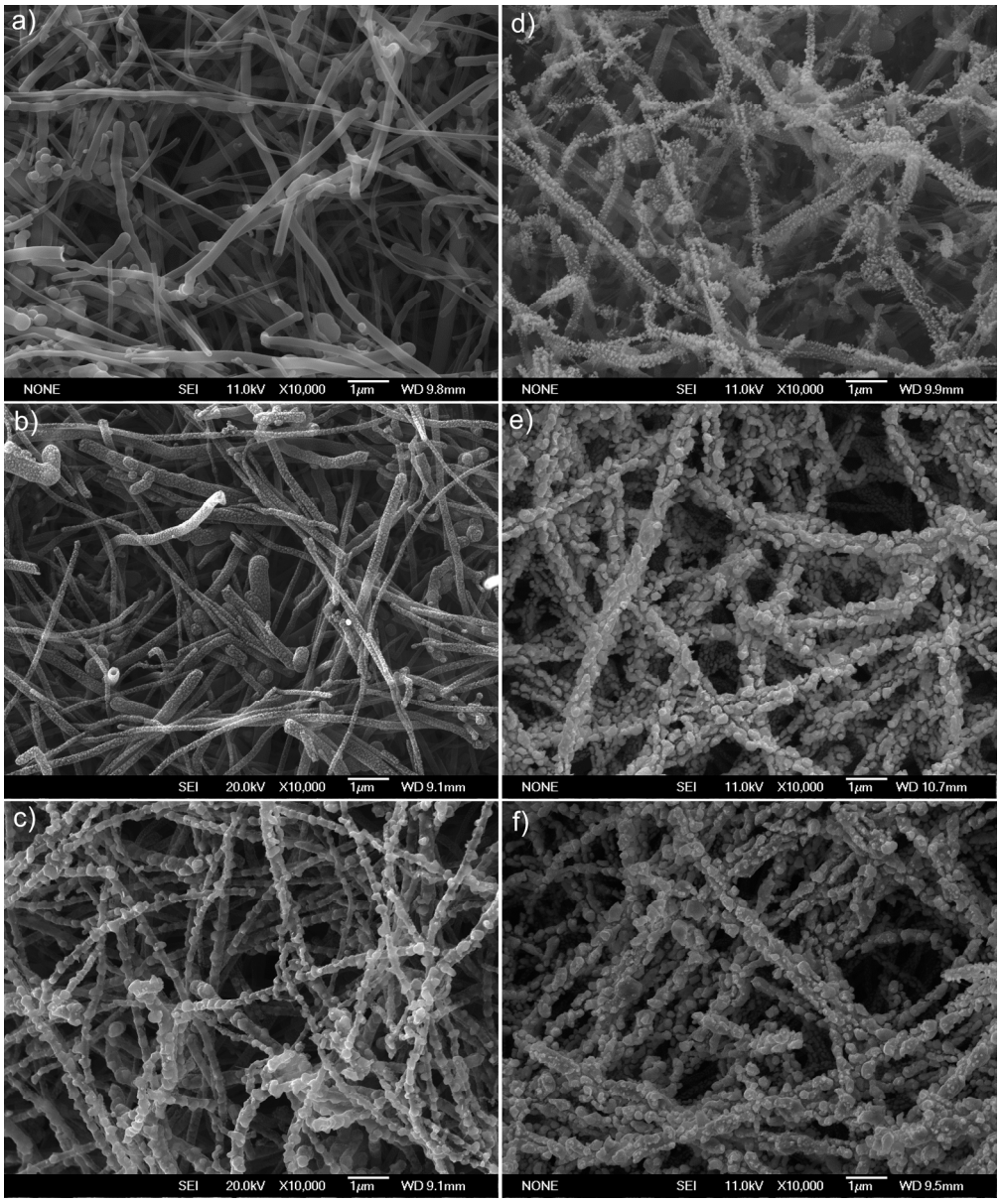

Figure 5. SEM micrographs of active screen plasma functionalized CNFs: AS(Ni): a) 15 min., b) 30 min., and c) 60 min.;AS(Ag): d) 30 min., e) 60 min., and f) 120 min.

577x694mm (96 x 96 DPI)

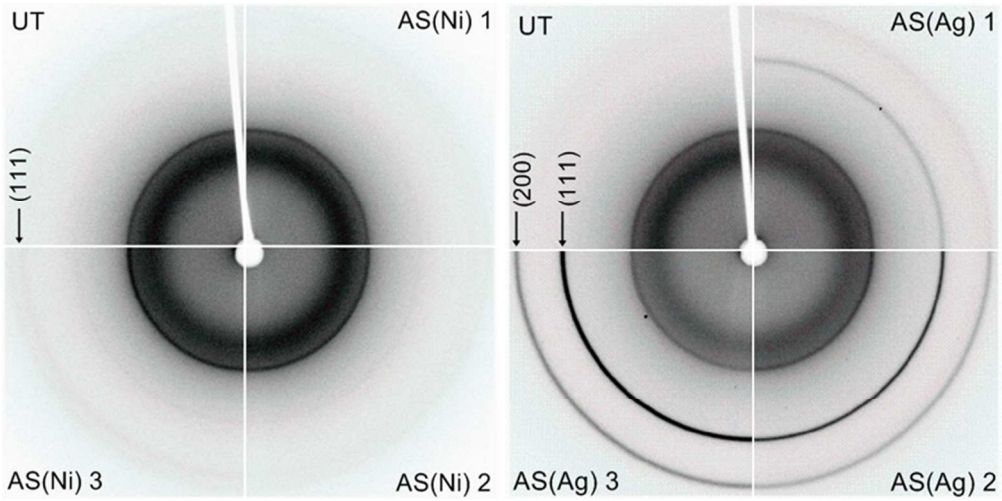

Figure 6. X-ray diffraction traces corresponding to: UT, AS(Ni) and AS(Ag) CNFs.

229x113mm (96 x 96 DPI)

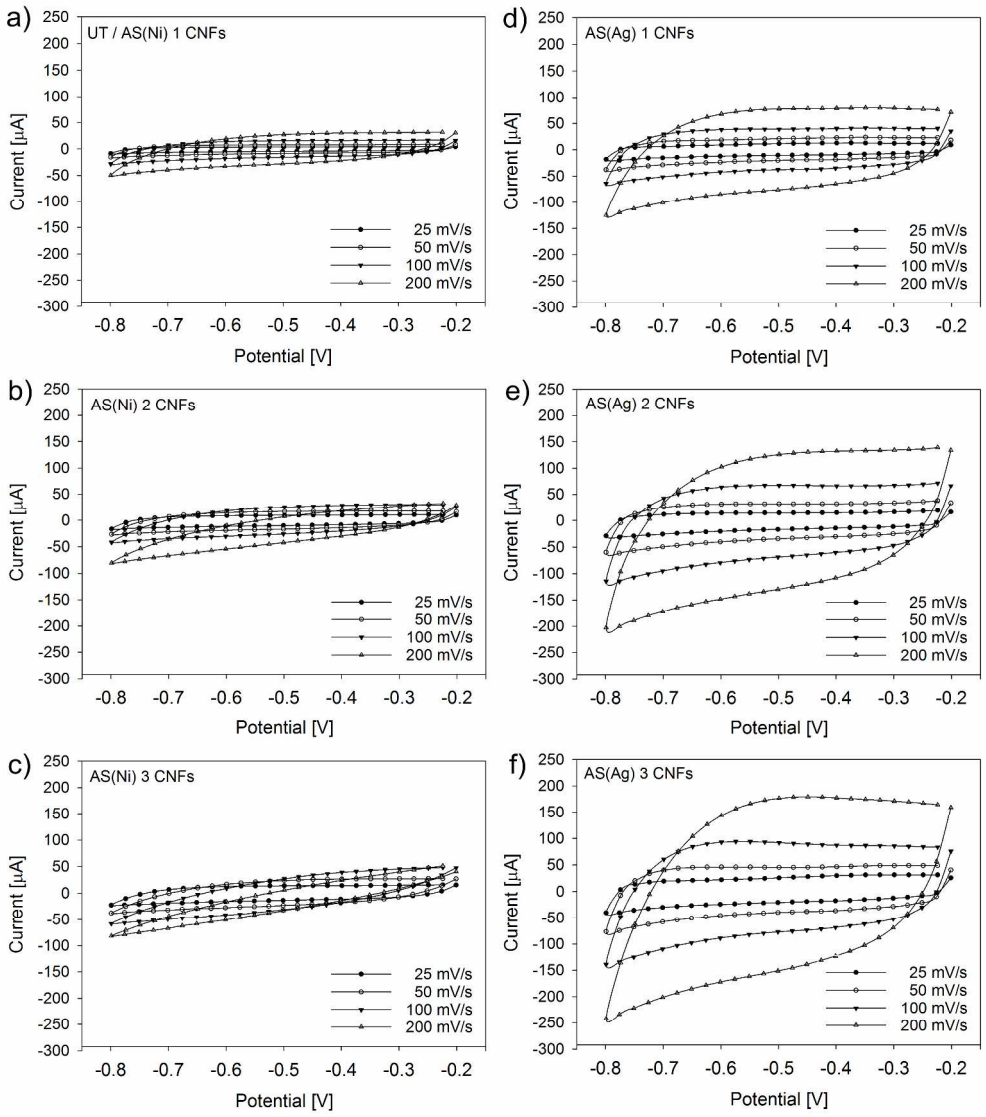

Figure 7. Cyclic voltammetry tests conducted on functionalized CNTs: a) UT / AS(Ni) 1, b) AS(Ni) 2, c) AS(Ni) 3, d) AS(Ag) 1, e) AS(Ag) 2 and f) AS(Ag) 3.

968x1090mm (96 x 96 DPI)

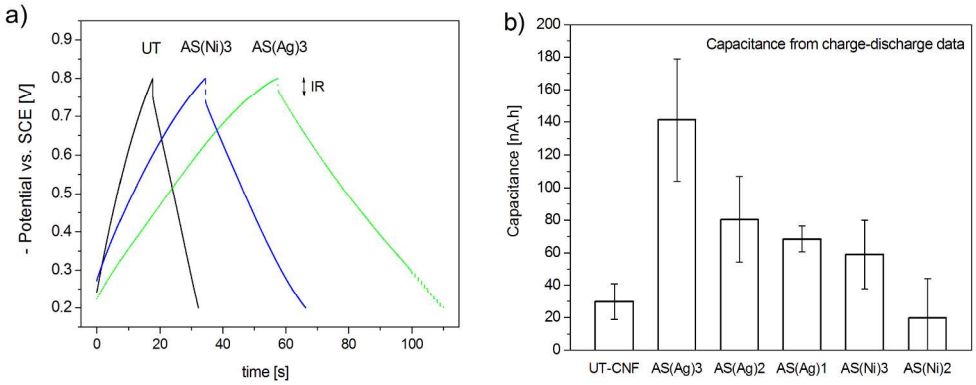

Figure 8. a) Cyclic charge-discharge curves (10 mA); and b) calculated capacity for CNFs with different surface conditions.

744x295mm (96 x 96 DPI)

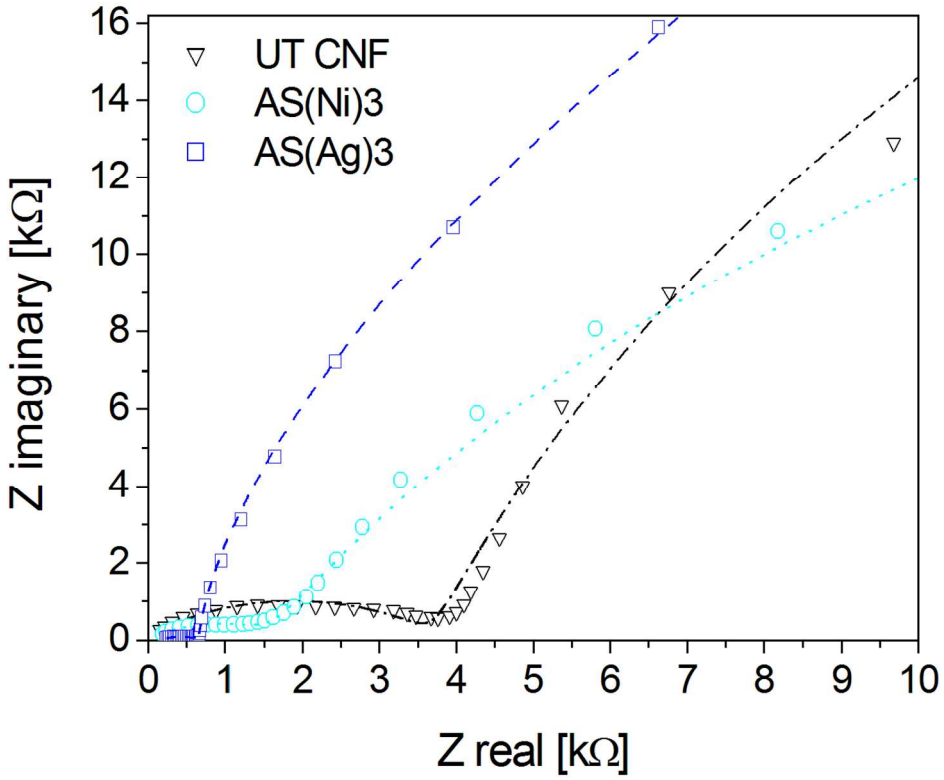

Figure 9. Electrochemical impedance spectra of UT, AS(Ni)3 and AS(Ag)3 CNF electrodes.

387x320mm (96 x 96 DPI)